RSC Advances

ROYAL SOCIETY OF CHEMISTRY

www.rsc.org/advances

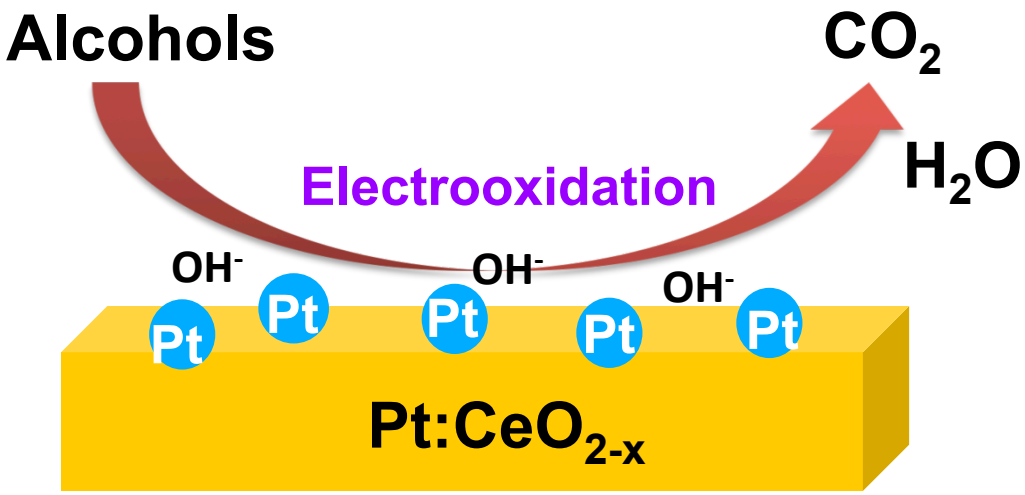

RSC Advances

RSCPublishing

ARTICLE

Preparation and characterization of Pt/Pt:CeO_{2-x} nanorods catalysts for small chain alcohol electrooxidation in alkaline media

Cite this: DOI: 10.1039/x0xx00000x

Received 00th January 2012,
Accepted 00th January 2012

DOI: 10.1039/x0xx00000x

www.rsc.org/

Christian L. Menéndez,[†, a] Yunyun Zhou,[†, b] Chris M. Marin,[b] Neil J. Lawrence,[b] E. Bryan Coughlin,[c] Chin Li Cheung[*,b] and Carlos R. Cabrera[*,a]

Multi-functional anode catalysts composed of platinum (Pt) nanoparticles electrodeposited on 2 wt.% Pt decorated ceria (Pt:CeO_{2-x}) nanorod supports were shown to enhance the alkaline electrocatalytic oxidation of methanol, ethanol and n-butanol over electrodeposited Pt nanoparticles alone or ones supported with pure ceria nanorods. The Pt:CeO_{2-x} nanorods support was demonstrated to increase the current density of the investigated alkaline electrooxidation of methanol, ethanol and n-butanol by more than 30 % over the other two catalysts.

1. Introduction

Fuel cells are efficient and low-to-zero pollutant emission sources of energy which have a wide range of potential applications in transportation vehicles and portable devices.[1] Alkyl alcohols with short carbon chains such as methanol, ethanol and n-butanol have been commonly proposed as alternative fuels because they possess higher energy density per weight when compared to gas fuels.[2] Among the direct alcohol fuel cells (DAFCs), direct methanol fuel cells (DMFC) have been extensively studied and evaluated for vehicle transportation applications partially because of the ease of large scale industrial methanol production.[3] The bio-renewable nature of ethanol and its lower toxicity make it as another attractive alternative of alcohol fuels.[4, 5] Though the energy densities of ethanol is 30+% higher than that of methanol (8.01 kWh kg^{-1} versus 6.09 kWh kg^{-1}),[6] the current efficiency of direct ethanol fuel cells reported in literature is typically less than those observed with direct methanol fuel cells. Despite the fact that n-butanol has even higher energy density (9.95 kWh kg^{-1}), comparable to that of petrol fuel,[7] the reported performances of n-butanol in direct fuel cells are generally even poorer. The major reasons for the lower performances of ethanol and n-butanol are commonly attributed to the severe difficulty to break the C-C bonds in these short carbon chain structures and the poisoning of noble metal catalysts used in traditional DAFC designs.[8]

To mitigate the poisoning of commonly used platinum (Pt) catalysts in fuel cells, various oxide promoters such as WO_3,[9] TiO_2,[9] Ta_2O_5,[10] NbO_2[11] and CeO_{2-x}[12] have been studied. These oxides were designed to support the Pt catalyst and assist oxidizing catalyst poisons such as carbon monoxide and other partially oxidized carbonaceous by-products from the alcohol electrooxidation process. Cerium oxide (ceria, CeO_{2-x}, $0<x\leq0.5$) is one of the promising promoter oxides[13-15] due to its high oxidizing power and its excellent oxygen storage and release ability to abate these by-products.[8, 15, 16] Ceria are typically applied as embedded materials in composites with platinum, platinum-ruthenium, platinum-carbon catalysts.[17-21] Various methods of fabricating Pt-ceria composite anodes have been employed, such as occlusion deposition,[22] chemical vapor deposition,[23] sputtering[24] and "catalyst paste" mixtures of metal precursors, support and conducting polymers.[25] Since different shapes of nanostructured ceria possessed different oxidizing power based on the density of oxygen vacancy defects,[26-28] many different shapes of ceria catalyst, including nanoparticles,[22] nanorods[29] and nanowires[30] have been studied. Ceria nanorods were found to possess larger density of oxygen vacancy defects and exhibit higher catalytic activity towards reactions, such as CO oxidation.[31]

Preparation methods and pre-treatments of Pt-ceria catalysts are critical in altering their resulting structures, chemical states and hence catalytic performance. For example, Ou et al. recently reported that annealing of Pt decorated polycrystalline ceria nanorods support in hydrogen could promote Pt nanoparticles to "invade" into the ceria structure and create a composite of smaller nanocrystalline ceria particles decorating

on the Pt particles.[32] The "invasion" of Pt in the ceria support under highly reducing environment suggests that more gentle catalyst preparation process for ceria supported Pt catalysts should be further explored.

Literature reports investigating the performance of Pt-ceria catalyst on alcohol electrooxidation reveal that the optimum Pt/ceria molar ratio of this catalyst system varies significantly for different alcohol fuels.[33] Importantly, such an optimum ratio was found to strongly depend on the Pt-ceria interaction, which is significantly impacted by the catalyst preparation methods. Since ceria is a wide band gap semiconductor and has low current conductance, a large content of pure ceria in the catalyst generally is expected to suppress the current produced from alcohol electrooxidation because of the increase in electrode resistance and the blocking of platinum catalytic sites.[34] Nonetheless, few literatures focused on studying the impedance effect of ceria support to seek to improve the effectiveness of the Pt-ceria catalyst system.

Herein we report a multi-functional composite catalyst made of platinum nanoparticles supported on 2 wt.% Pt decorated CeO_{2-x} nanorods for the electrooxidation of methanol, ethanol and n-butanol in alkaline media. Our study focuses on using an anode "ink paste" composite catalyst composed of 2 wt.% Pt decorated ceria ($Pt:CeO_{2-x}$) nanorods, electrochemically deposited Pt nanoparticle clusters and conducting polymers. (Fig. 1a) The composite catalysts (abbreviated as $Pt/Pt:CeO_{2-x}$) were synthesized by a multi-step method. The $Pt:CeO_{2-x}$ nanorods were synthesized using an adapted hydrothermal method, followed by wet impregnation of platinum salts to increase their electrical conductivity.[28] Pt nanoparticles were then electrochemically synthesized and deposited at a controlled potential onto glassy carbon (GC) electrodes pre-coated with a catalyst "ink-paste" composed of $Pt:CeO_{2-x}$ nanorods and Fumion® polyelectrolytes. Highly crystalline ceria nanorods were chosen over other nanostructures because it was reported to have higher oxidizing power when thermally activated under low pressure.[28] Composite catalysts of Pt nanoparticle clusters and $Pt:CeO_{2-x}$ nanorods were further demonstrated in enhancing the efficiency of direct alcohol oxidation over similarly prepared anode catalysts with pure ceria nanorods and also the Pt nanoparticles catalyst. These findings provide further perspectives on increasing the electrical conductance of the promoter oxide and thus improvement of the direct electrooxidation of alcohols.

2. Experimental method

2.1 Preparation of 2 wt.% Pt decorated ceria ($Pt:CeO_{2-x}$) nanorods and CeO_{2-x} nanorods

2 wt.% $Pt:CeO_{2-x}$ nanorods were prepared using a modified hydrothermal procedure for synthesizing ceria nanorods.[28] A mixture of 0.5 g of cerium (III) sulphate and 40 mL of 10 M sodium hydroxide in a 50-mL capacity Teflon-lined stainless steel autoclave was hydrothermally treated at 120 °C for 15 h. in a convection oven to produce cerium (III) hydroxide nanorods. The filtered product was rinsed with three aliquots of 50 mL of water and then placed in a convection oven for another 2 h. at 50 °C for further oxidation. Subsequently, 25 mL of water, and 1.536 mL of 0.02 M potassium tetrachloroplatinate(II) (K_2PtCl_4) solution were mixed with the nanorods and stirred for 20 min. Afterwards, 25 mL of 30 % aqueous hydrogen peroxide was added to the mixture and sonicated for 30 min., followed by mechanical stirring for an additional 30 min. to achieve complete reaction. The resulting products were filtered, rinsed with three aliquots of 50 mL of 18 MΩ·cm deionized water, and dried for 4 h. at 50 °C in a convection oven. Before use, the synthesized materials were activated at 400 °C in a flow of 100 SCCM (standard cubic centimeter per minute) of simulated air (20 % O_2/ 80 % N_2) for 30 min. in a horizontal quartz tube furnace at an operating pressure of 2.0 Torr.

2.2 Preparation of catalyst coated glassy carbon (GC) electrodes

Coating of Pt nanoparticles/$Pt:CeO_{2-x}$ nanorods ($Pt/Pt:CeO_{2-x}$) catalyst onto glassy carbon (GC) electrodes was accomplished using a two-step process. For the first step, the catalyst "ink" paste mixture was made by mixing 1 mg of 2 wt.% $Pt:CeO_{2-x}$ nanorods, 100 µL of nanopure water of 18 MΩ·cm resistivity, 200 µL of isopropanol, and 8 µL of Fumion® (5 % w/w polyarylene sulfonic acid polyelectrolyte dissolved in water/isopropanol, FuMA-Tech GmbH, St. Ingbert, Germany). Afterwards, the "ink" mixture was sonicated for 60 s and stirred for 10 min. to increase its composition uniformity. 8 µL of the "ink" paste was then drop-casted onto the surface of a clean GC electrode. Typically, the deposited "ink" dried on the electrode after 30 min. of exposure to ambient conditions. For the second step, Pt nanoparticles were electrodeposited to the modified GC electrode by applying a constant potential of -0.200 V vs. Ag/AgCl for 30 s at room temperature while the electrode was immersed in an aqueous 1 mM K_2PtCl_6/ 0.5 M H_2SO_4 solution.

Coating of Pt nanoparticles/CeO_{2-x} nanorods (Pt/CeO_{2-x}) catalyst onto GC electrodes for the control experiments was performed similarly as that for the $Pt/Pt:CeO_{2-x}$ coated GC electrodes except that CeO_{2-x} nanorods were used instead. Pt nanoparticles coated GC electrodes were fabricated by electrodepositing Pt nanoparticles to a modified "ink" paste (without 1 mg CeO_{2-x} nanorods catalyst) deposited GC electrodes by applying a constant potential of -0.200 V vs. Ag/AgCl for 30 s at room temperature while the electrodes were immersed in aqueous 1 mM K_2PtCl_6/ 0.5 M H_2SO_4 solutions.

2.3 Catalyst morphology, structure and composition characterization

The structure and chemical identity of the 2 wt.% $Pt:CeO_{2-x}$ nanorods was studied by transmission electron microscopy (TEM), energy dispersive X-ray spectroscopy (EDX), X-ray powder diffraction (XRD), inductive coupled plasma optical emission spectroscopy (ICP-OES) and X-ray photoelectron spectroscopy (XPS). TEM micrographs and selected area electron diffraction of the samples were obtained using a Tecnai G^2 F20 S-Twin field-emission TEM operated at 200 kV (FEI Company, Hillsboro, OR). The EDX spectra of the imaged sample were determined with an Oxford Instruments EDX system (Oxford Instruments, Oxfordshire, UK). The crystal structures of the nanorods were examined with a Bruker Discover D8 (Bruker AXS, Madison, WI). The XRD instrument was equipped with a Cu Kα X-ray source of average wavelength 1.544 Å. Elemental composition of the 2 wt.% $Pt:CeO_{2-x}$ nanorods was analyzed using a Thermo Jarrell Ash IRIS Advantage Inductively Coupled Plasma Optical Emission Spectrometer. The XPS analysis of the nanorods was performed using a PHI 5600ci spectrometer equipped with a hemispherical electron analyser and a

monochromatic Al Kα X-ray source operated at 15 kV and 350 W. The recorded binding energy data was calibrated using the carbon 1s peak. The software XPSPEAK was used for the Pt 4*f* XPS data fitting analysis.

The morphology of the catalysts-coated GC electrodes was investigated using a scanning electron microscope (SEM) operated at 2 to 5 kV (Hitachi High Technologies America, Inc., Pleasanton, CA). Elemental mapping of the catalysts-coated electrodes was obtained using a FEI Nova NanoSEM450 **(**FEI Company, Hillsboro, OR) operated at 20 kV and equipped with an Oxford Instruments EDX system (Oxford Instruments, Oxfordshire, UK).

2.4 Cyclic voltammetry and constant potential experiments

All cyclic voltammetry (CV) experiments were performed in a 3-electrode conventional electrochemical cell using a potentiostat (Electrochemical System PARC EG&G Instruments and CHI Model 1200B) by applying a direct current voltage at 100 mV/s vs. Ag/AgCl at room temperature. The counter electrode was a Pt wire. All electrolyte solutions were bubbled with argon gas for 10 min. before use. The active surface areas of platinum on the catalyst coated anodes (working electrodes) were calculated from the cyclic voltammograms in 0.1 M KOH solutions using the adsorption/desorption of hydrogen method. The half-cell studies were performed in 1 M alcohol (methanol, ethanol or n-butanol)/ 0.1 M KOH solutions. The controlled potential experiments to study the catalytic activity of the composites were performed at the onset potential in 1 M alcohol/ 0.1 M KOH solution as well.

2.5 CO stripping experiment

For the CO stripping experiment in alkaline medium, the electrodes were placed in a solution of 0.1M KOH using an Ag/AgCl reference electrode and a Pt wire as the counter electrode. The first step was to bubble high purity N_2 gas to purge the solution for 20 min. Then, CO gas was bubbled into the solution at a potential of -0.7 V vs. Ag/AgCl for 10 min. Afterwards, the potential of -0.7 V vs. Ag/AgCl was applied while high purity N_2 gas was bubbled to purge the remaining CO present in solution. The final step was to perform a linear sweep voltammetry (LSV) from -0.7 V to 0.7 V vs. Ag/AgCl with a sweep rate of 20 mV/s.

3. Results and discussion

3.1 Morphology, structure and chemical composition of anode catalysts

The structure and chemical identity of 2 wt.% Pt:CeO_{2-x} nanorods were verified by our TEM and XRD studies. From the TEM images in Fig. 1a, the as-synthesized materials were found to have nanorod shapes with diameters of 10-20 nm and lengths of 30-200 nm. Fig. 1b shows the XRD diffraction pattern for the 2 wt.% Pt:CeO_{2-x} catalysts. The XRD pattern exhibited fluorite crystal structure similar to that of cerium(IV) oxide (CeO_2).[35] Neither platinum, platinum hydroxide nor platinum oxide species were revealed by our TEM or XRD data, likely due to the well-dispersion of platinum on the ceria nanorods and the detection limit of these techniques. Nonetheless, ICP-OES analysis verified the weight percentage of Pt to be 2 wt.% in the Pt:CeO_{2-x} nanorod samples.

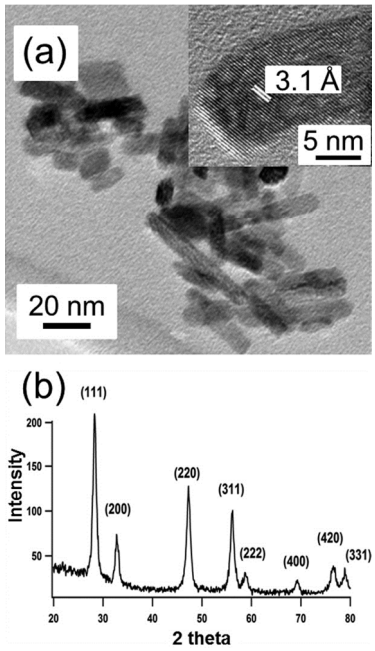

Fig. 1 (a) TEM image of 2 wt.% Pt:CeO_{2-x} nanorods. (Inset) High-resolution TEM image of one nanorod. (b) XRD pattern of the Pt:CeO_{2-x} nanorods (Peaks indexed against fluorite-structured ceria)

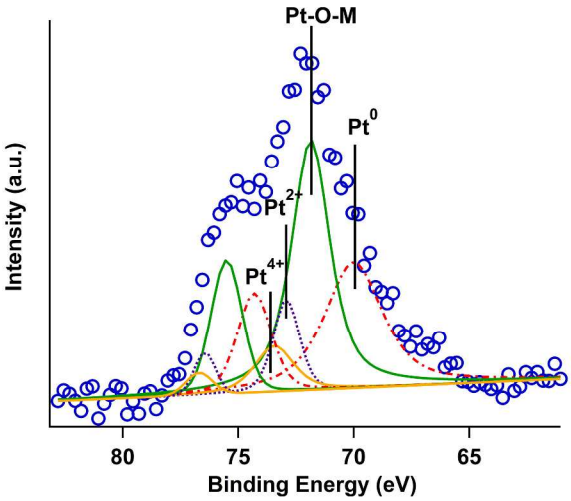

Fig. 2 X-ray photoelectron spectra and fitting analysis of Pt 4*f* binding energy regions for 2 wt.% Pt:CeO_{2-x} nanorods.

The deposited Pt forms different species on the surface of the ceria nanorods support. The Pt species also modifies the ceria nanorods due to the strong metal support interaction. The XPS spectrum of 2 wt.% Pt:CeO_{2-x} nanorods has two spin-orbit splitting doublets Pt $4f_{7/2}$ and $4f_{5/2}$. The peaks at 70.5 eV and 72.9 eV binding energies were attributed to Pt^0 and Pt^{2+} states, respectively.[36] (Fig. 2) The peak at 71.9 eV was assigned to Pt-O-M peak which corresponds to slightly ionized Pt. M has been assigned to be either a Ce cation or an oxygen vacancy site.[37] At the binding energy of 73.4 eV, a small peak was fitted according to Pt^{4+}. The fitting analysis of the Pt 4*f* spectrum suggests that the Pt species on the ceria nanorods were composed a significant portion of Pt^0 states (36%) and Pt-O-M states (46%). Small percentages of Pt species are in the states of Pt^{2+} (10%) and Pt^{4+} (8%).

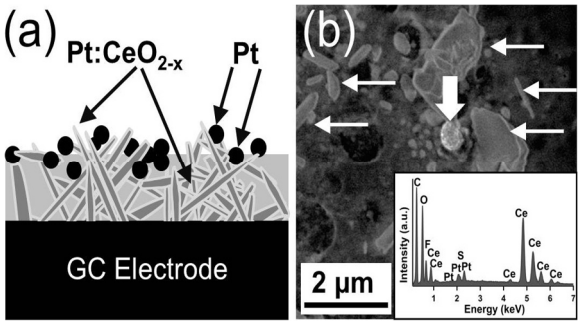

Fig. 3 (a) Cross-sectional schematic of Pt/Pt:CeO_{2-x} catalyst coating on a glassy carbon (GC) electrode. (rods) Pt:CeO_{2-x} nanorods, (black circles) electrodeposited Pt nanoparticle clusters and (light grey) Fumion® polymeric conductor layer. (b) SEM image of an electrocatalyst Pt/Pt:CeO_{2-x}/ Fumion® coating on a glassy carbon electrode. (Thin arrows: Pt/Pt:CeO_{2-x} catalyst clusters; thick arrows: Pt nanoparticle clusters)

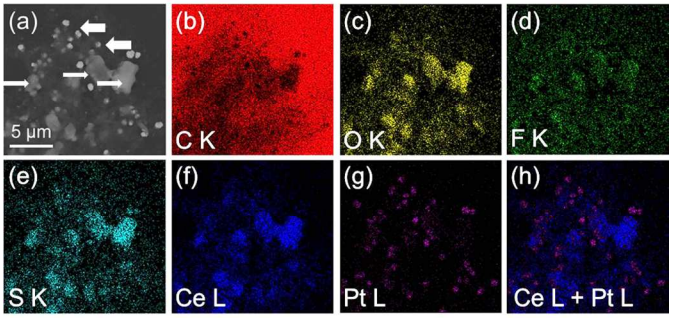

Fig. 4 (a) SEM image of an electrocatalyst Pt/Pt:CeO_{2-x}/ Fumion® coating on a glassy carbon electrode. (Thin arrows: Pt/Pt:CeO_{2-x} catalyst clusters; thick arrows: Pt nanoparticle clusters) EDX elemental mapping of (b) carbon (red), (c) oxygen (yellow), (d) fluorine (dark blue), (e) sulfur (cyan), (f) cerium (green) and (g) platinum (magenta) of the catalyst coating in (a). (h) Combined mapping image of both Ce and Pt. The X-ray signals indicating the presence of fluorine and sulfur are from the Fumion® polyelectrolyte.

Fig. 3a is a schematic representation of the final composite electrode with an ink paste and platinum electrodeposited nanoparticles. The surface morphology of the Pt/Pt:CeO_{2-x} catalyst coating on a GC anode typically displays complex structures of Pt nanoparticle clusters among Pt:CeO_{2-x} nanorods/Fumion® "ink paste". Under SEM, the "ink paste" of Pt:CeO_{2-x} nanorods often existed as either rod or irregularly shaped structures with sizes ranging from a few 100 nanometers to a few microns as indicated by thin arrows in Fig. 3b. The agglomeration of Pt:CeO_{2-x} nanorods to form larger particles were likely promoted by the Fumion® polymer. The electrochemically deposited clusters of Pt nanoparticles have diameters of 100 to 600 nm and are dispersed on the top of the catalyst coating. (Thick arrows in Fig. 3b) The size distribution is similar to those of electrodeposited Pt nanoparticles on only Fumion® coated GC electrodes. (Data not shown) The presence and distribution of platinum, cerium and oxygen in this catalyst composite coating is confirmed by EDX elemental mapping analysis. (Fig. 4) The fluorine and sulfur signatures verify the presence of the Fumion®.

3.2 KOH cyclic voltammetry and surface area determination

Fig. 5 shows the CV in 0.1 M KOH for the platinum (Pt nanoparticles), Pt/Pt:CeO_{2-x} and Pt/CeO_{2-x} composite electrodes. The platinum surface of platinum nanoparticles

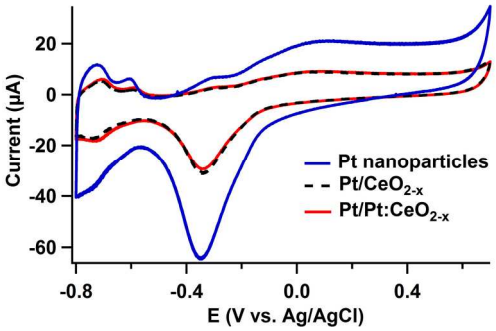

Fig. 5 Cyclic Voltammetry at 100 mV/s in 0.1 M KOH for the final composite electrodes. Initial potential was -0.5 V vs. Ag/AgCl. Total number of cycles = 10. Note that the CV data of Pt/CeO_{2-x} coated electrodes (dotted line) almost overlaps that of the electrode coated with Pt/Pt:CeO_{2-x} (black line).

electrode is higher than those of Pt/Pt:CeO_{2-x} and Pt/CeO_{2-x} electrodes. This is likely ascribed to the fact that the presence of ceria makes the GC surface less conductive. This caused difficulties in depositing platinum and resulted in fewer platinum nanoparticles that contribute to the total surface area.

Table 1 Platinum loadings, platinum percentage and platinum surface areas of three catalyst-coated glassy carbon working electrodes.

Catalysts	Loading (µg of Pt)	Wt.% Pt	Surface Area (cm^2 of Pt)
Pt/CeO_{2-x}	1.53	5.6	0.031
Pt/Pt:CeO_{2-x}	1.69	6.1	0.039
Pt only	2.31	8.2	0.095

Table 1 shows the Pt loading, the Pt weight percentage and the Pt surface area for the three different kinds of catalyst-deposited GC electrodes. The final platinum loadings on the electrodes were calculated by integrating the current–time curves used for the Pt electrodeposition with the Faraday law and accounting for the contributions of the 2 wt.% Pt content from the Pt:CeO_{2-x} nanorods. All dilution factors were taken in considerations in the calculations of the final Pt loadings on these evaluated electrodes. Among all three electrodes, the electrode with only Pt nanoparticles have the highest Pt loading, wt.% of Pt and active surface area of Pt. Comparing the data for the two composite-catalyst coated electrodes with ceria nanorods, the additional contribution of Pt from decorated Pt on the ceria nanorods only increases 0.5 total wt.% of Pt in the final catalyst-composite.

3.3 Methanol electrooxidation

Our cyclic voltammetry study indicates that the Pt/Pt:CeO_{2-x} catalyst consistently outperformed with anode catalysts composed of similar "ink paste" than with pure CeO_{2-x} nanorods (Pt/CeO_{2-x}) or just platinum nanoparticle clusters towards the electrooxidation of methanol. (Fig. 6a) CVs of methanol oxidation using these three anode catalysts typically displayed the peak potential (E_p) at about 0.05 V vs. Ag/AgCl. The onset potential (E_s) for methanol oxidation is at -0.35 V vs. Ag/AgCl which are consistent with the Pt/ceria catalyzed methanol oxidation in literature.[18]

The maximum current densities of the three catalysts are 18.5 (Pt/Pt:CeO_{2-x}), 17.5 (Pt/CeO_{2-x}), and 11.5 mA/ cm^2 of Pt (Pt nanoparticle clusters), respectively. The order of these

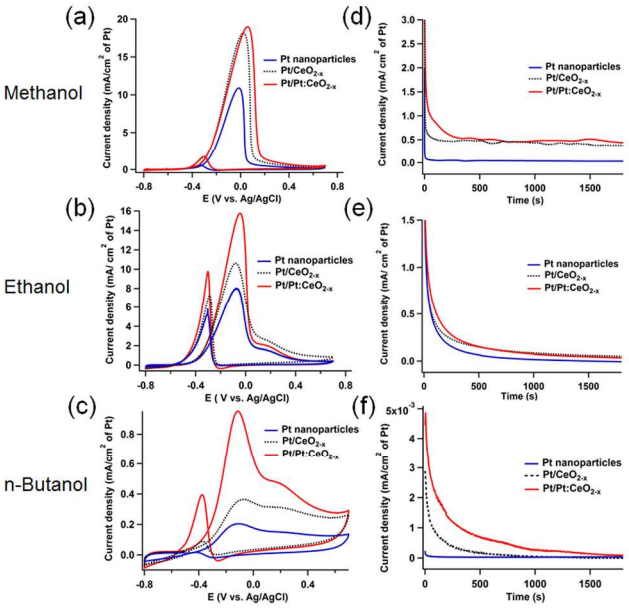

Fig. 6 Electrochemical characterization of glassy carbon electrodes coated with platinum nanoparticles, platinum nanoparticles/CeO_{2-x} nanorods (Pt/CeO_{2-x}), or platinum nanoparticles/2 wt.% $Pt:CeO_{2-x}$ nanorods ($Pt/Pt:CeO_{2-x}$) for the electrooxidation of methanol (a and d), ethanol (b and e) and n-butanol (c and f) in 0.1 M KOH at 100 mV/s. (a-c) Cyclic voltammograms; (d-f) chronoamperometric responses at a potential of -350 mV vs. Ag/AgCl.

catalysts performances was consistent with three other trials of experiments. Xu et al[34] postulated that ceria support functions a similar bifunctional role as that of ruthenium (Ru) in Pt-Ru/C catalysts. Oxygen-rich species such as hydroxyls adsorbed on the ceria surface may transfer to the surface of Pt poisoned with adsorbed CO-like species, transform the CO species into gaseous CO_2, and free up more Pt surface catalytic sites for further alcohol electrooxidation. Fig. 7a shows the LSVs of the methanol oxidation at 1 mV/s for the three composite electrodes. The idea of using this small sweep rate is to minimize the contribution of the double layer current and maximize the contribution of faradic current. The electrode with $Pt/Pt:CeO_{2-x}$ catalyst demonstrated the lowest onset potential, followed by Pt/CeO_{2-x} and platinum nanoparticles electrodes. This indicates that the $Pt/Pt:CeO_{2-x}$ catalyst is the most catalytic active one towards methanol oxidation among the three evaluated catalysts.

Chronoamperometry responses from the $Pt/Pt:CeO_{2-x}$, Pt/CeO_{2-x}, and Pt nanoparticles catalysts were obtained to determine the stability of catalysts during the alcohol electrooxidation. Fig. 6d shows that the obtained current densities for methanol oxidation were stable for at least 1800 s for the half-cell study with the $Pt/Pt:CeO_{2-x}$ and Pt/CeO_{2-x} anode catalyst. However, the anode with Pt nanoparticle clusters yielded a shorter stable period and much lower current density, 0.02 mA/cm^2 of Pt compared with 0.5 mA/cm^2 obtained from the $Pt/Pt:CeO_{2-x}$ and Pt/CeO_{2-x} anode catalysts. This is likely because Pt particles are more susceptible to the poisoning of CO by-product produced during the methanol electrooxidation. The better performance of the $Pt/Pt:CeO_{2-x}$ and Pt/CeO_{2-x} catalysts in comparison to the Pt nanoparticles catalyst is attributed to the poisoning resistance of the composite catalysts. Likely, the ceria support functions similarly as ruthenium in the composite catalyst, which promotes the CO oxidation by providing oxygen-rich species to the Pt surface.[19]

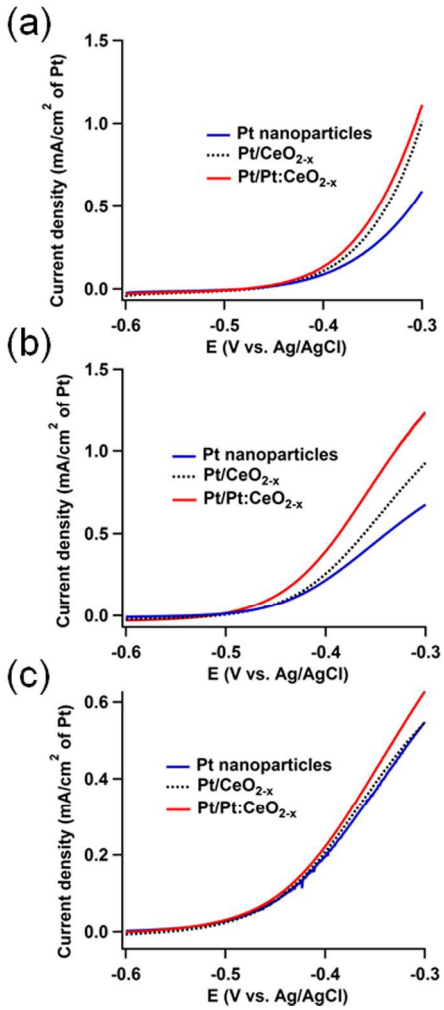

Fig. 7 Onset potentials of alcohol electrooxidation for the $Pt/Pt:CeO_{2-x}$, Pt/CeO_{2-x} and Pt only electrode catalysts at 1 mV/s. (a) 1 M methanol/ 0.1M KOH, (b) 1 M ethanol/ 0.1 M KOH and (c) 1 M n-butanol/ 0.1 M KOH.

3.4 Ethanol electrooxidation

Ethanol is a popular bio-renewable alcohol-based fuel.[38] CVs of ethanol oxidation using these three anode catalysts typically displayed two major oxidation peaks at -0.35 V and -0.08 V vs. Ag/AgCl. (Fig. 6b) The current densities at -0.08 V are 7.8 mA/cm^2 for Pt nanoparticles, 10.2 mA/cm^2 for Pt/CeO_{2-x} and 15.5 mA/cm^2 for $Pt/Pt:CeO_{2-x}$, respectively. The $Pt/Pt:CeO_{2-x}$ catalyst yielded almost two times higher current density than that of pure Pt nanoparticles coated anode. However, these current densities are smaller than the ones obtained for methanol. Fig. 7b shows the LSV ethanol electrooxidation in 1 M ethanol/ 0.1M KOH solution at 1 mV/s. The onset potential decreases in this corresponding order: Pt nanoparticles > $Pt:CeO_{2-x}$ > $Pt/Pt:CeO_{2-x}$. Again, the $Pt/Pt:CeO_{2-x}$ composite is the most active catalyst in oxidizing ethanol thermodynamically among the three evaluated anode catalysts. Chronoamperometric responses for the ethanol system are shown in Fig. 6e. The results are also consistent with the LSV data and the CV electrooxidation experiment.

3.5 n-Butanol electrooxidation

n-Butanol, though has comparable energy density to petro fuel, has not been demonstrated as a viable fuel source because of the severe difficulty to fully electrochemically oxidize this chemical and extract the thermodynamically predicted energy content. All three catalyst systems showed about 10x smaller but noticeable current density in the half-cell study. The CVs of n-butanol oxidation using these three anode catalysts typically displayed three major oxidation peaks at -0.4 V, -0.05 V and 0.1 V vs. Ag/AgCl. (Fig. 6c) The onset potential for the electrooxidation of n-butanol and the associated current density for Pt/Pt:CeO_{2-x} coated anodes are -530 mV vs. Ag/AgCl and 0.950 mA/cm^2, whereas those for Pt nanoparticle clusters anodes are -402 mV vs. Ag/AgCl and 0.203 mA/cm^2, respectively. The 100 mV difference between the two values of E_s for the anodic reaction is significant in DAFCs. The decrease of E_s with Pt/Pt:CeO_{2-x} coated anodes indicated that the activity for n-butanol oxidation was higher than the other two catalysts by improvement of kinetics.[39] The chronoamperometric responses (Fig. 6f) from these three catalysts coated anodes yield very low current, suggesting the poor oxidative ability of n-butanol with these catalysts. However, the Pt/Pt:CeO_{2-x} coated anodes exhibit the slowest decay rate in current density, which implies the poisoning abating effect of Pt:CeO_{2-x} in this reaction. In the LSV data in 1 M n-butanol/ 0.1 M KOH solution, (Fig. 7c) the electrode with Pt:Pt/CeO_{2-x} catalyst again demonstrated the lowest onset potential, and the trend is the same as those in methanol and ethanol solutions. This indicates that the Pt:Pt/CeO_{2-x} catalyst is the most catalytic active one towards n-butanol oxidation among the three evaluated catalysts.

3.6 Effect of Pt:CeO_{2-x} promoter oxide support on the electrooxidation of small chain alcohols

Among the three evaluated alcohol electrocatalysts, Pt/Pt:CeO_{2-x} exhibited higher catalytic performance than those of Pt nanoparticles and Pt/CeO_{2-x}. Interestingly, the relative enhancement in electrocatalytic activity for Pt/Pt:CeO_{2-x} for n-butanol oxidation is higher than those for methanol and ethanol electrooxidation when compared with Pt:CeO_{2-x} and pure Pt nanoparticles coated anodes. In methanol oxidation, the enhancement factors are 1.06 and 1.23 for Pt:CeO_{2-x} and pure Pt nanoparticles, respectively. In ethanol oxidation, the corresponding values are 1.52 and 1.99. In contrast, for n-butanol oxidation, the enhancement factors are 2.96 and 4.75.

The distinct improvements are likely due to the presence of 2 wt.% of Pt in the CeO_{2-x} nanorods, which might had enhanced the electrical conductivity of CeO_{2-x} nanorods Better conductive catalysts are expected to result in less resistance and thus more efficient electrooxidation. Doping the ceria with metal ions can increase the ionic conductivity.[40] In our case, from our XPS study, most of the Pt species in the 2 wt.% Pt decorated on the ceria nanorods are in the form of Pt^0 (36 %) and Pt-O-M (46 %) which corresponds to slightly ionized Pt. See Fig. 2) The large percentage of Pt species in the Pt-O-M indicates strong interactions between Pt and the ceria support. Such strong interactions likely lead to changes in the electronic structure of the Pt:CeO_{2-x} and its crystal lattice distortion, which will affect the ionic conductivity of ceria.[41] According to(previous studies, dopants are often reported to increase the electrical conductivity of ceria support and promote its use as anode materials.[42, 43] The considerable proportion of Pt species in the Pt^0 state on ceria surface can possibly provide another

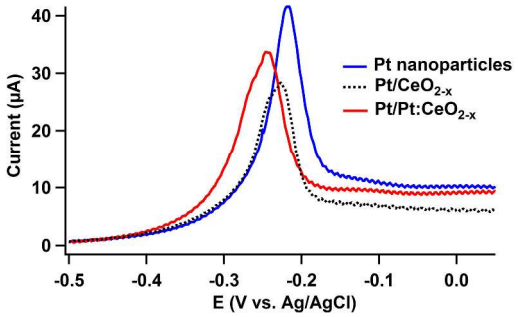

Fig. 8 Variation of the potential of CO stripping with Pt/Pt:CeO_{2-x}, Pt/CeO_{2-x} and Pt only electrode catalysts in 0.1M KOH. All CO stripping data was recorded at 20 mV/s from -0.7 V to 0.7 V vs. Ag/AgCl.

pathway to enhance the conductivity of Pt:CeO_{2-x} catalyst during the electrochemical reaction. Hence, the catalyst with Pt decorated ceria deposited on the electrode (Pt/Pt:CeO_{2-x}) is likely more conductive and with smaller impedance for facilitating the current transfer from solution to the electrode. The ceria nanorods in the composite catalysts functioned to remove catalyst poisoning as well boosting the catalytic activity of Pt/Pt:CeO_{2-x} catalysts. Our results revealed that the catalytic activity of the "ink paste" composite catalyst can be increased significantly with only a small percentage (2 wt.%) Pt decorated on the ceria support.

3.7 CO stripping experiment

To evaluate the effect of Pt:CeO_{2-x} nanorods and ceria nanorods in mitigating the CO poisoning of the platinum nanoparticles electrodeposited on the anode catalyst coatings, linear sweep voltammetry was used to strip the CO from these platinum nanoparticles of the three evaluated anode catalysts after they were saturated with CO gas. Since CO is a common by-product of alcohol electrooxidation, it is expected that the catalysts with better performance in alcohol electrooxidation will require lower potential to strip the adsorbed CO. Fig. 8 shows the CO stripping sweep voltammetry in alkaline medium (0.1 M KOH) for the prepared catalysts on the composite electrodes.

The CO stripping peak for the Pt nanoparticle clusters coated anode takes place at a potential of -217 mV vs. Ag/AgCl, which is a higher value than the potential of -227 mV and -248 mV vs. Ag/AgCl for the Pt/CeO_{2-x} and Pt/Pt:CeO_{2-x} catalysts coated anodes, respectively. All CO was removed during the first scan. Only the first scans are shown since the major interest is the shift in stripping potentials. Our data suggests that it is thermodynamically more favorable to electrooxidize CO to CO_2 in the presence of ceria than solely platinum nanoparticle clusters on GC electrodes without ceria coating. Ceria can promote CO removal by oxidation with oxygen stored in ceria's lattice.[44] The ability of ceria to release oxygen assists the Pt:CeO_{2-x}catalysts in carrying out the oxidation of CO to CO_2 and removing the adsorbed CO.[28, 36, 45]

Conclusions

An "ink paste" electrocatalyst composed of Pt:CeO_{2-x} was prepared and confirmed that the composite catalysts generate higher electro-oxidation current densities than the only Pt electrodes towards alkaline electrooxidation of small chain molecular alcohols (methanol, ethanol and n-butanol). The catalytic activity can be attributed to the presence of active

CeO_{2-x} support. CO stripping experiments showed that the desorption potential of CO depends on the composition of the composite electrode. The improvement in electrocatalytic responses of our catalyst for the oxidation of short-chained alcohols validates the critical use of high-activity oxidizing support with higher conductivity in designs of fuel cell anodes.

Acknowledgements

We thank the NASA-URC (NNX10AQ17A), NSF-EPSCoR (OIA-0701525), Army Research Office (W911NF-10-2-0099), NSF-NSEC Center for Hierarchical Manufacturing Grant No. (CHM-CMMI-053117) and US Army MURI on Ion Transport in Complex Heterogeneous Organic Materials (W911NF-10-1-0520) for financial support. J. Goodwin from the University of Alabama is acknowledged for help with the microscopy work. CLM is grateful to the University of Puerto Rico-DEGI and NSF-NSEC (CHM-CMMI-053117) for his scholarships.

Notes and references

[a] *Department of Chemistry and NASA-URC Center for Advanced Nanoscale Materials, University of Puerto Rico, Rio Piedras Campus, San Juan, Puerto Rico 00936, USA. E-mail: carlos.cabrera2@upr.edu*
[b] *Department of Chemistry and Nebraska Center for Materials and Nanoscience, University of Nebraska-Lincoln, Lincoln, NE 68588, USA. E-mail: ccheung2@unl.edu*
[c] *Polymer Science and Engineering Department, University of Massachusetts, Amherst, MA 01003, USA.*

† These authors contributed equally.

1. P. Waszczuk, J. Solla-Gullón, H. S. Kim, Y. Y. Tong, V. Montiel, A. Aldaz and A. Wieckowski, *J. Catal.*, 2001, **203**, 1-6.
2. Y. Ma, R. Wang, H. Wang and S. Ji, *Int. J. Electrochem. Sci.*, 2013, **8**, 6085 - 6093.
3. A. O. Neto, E. G. Franco, E. Aricó and M. Linardi, *Port. Electrochim. Acta*, 2004, **22**, 93-101.
4. C. Lamy, S. Rousseau, E. M. Belgsir, C. Coutanceau and J. M. Léger, *Electrochim. Acta*, 2004, **49**, 3901-3908.
5. S. Song, W. Zhou, Z. Zhou, L. Jiang, G. Sun, Q. Xin, V. Leontidis, S. Kontou and P. Tsiakaras, *Int. J. Hydrogen Energy*, 2005, **30**, 995-1001.
6. W. Zhou, *Appl. Catal. B*, 2003, **46**, 273-285.
7. N. Savage, *Nature*, 2011, **474**, S9-11.
8. A. Tabet-Aoul and M. Mohamedi, *Phys. Chem. Chem. Phys.*, 2012, **14**, 4463-4474.
9. J. Shim, C.-R. Lee, H.-K. Lee, J.-S. Lee and E. J. Cairns, *J. Power Sources*, 2001, **102**, 172-177.
10. O. A. Baturina, Y. Garsany, T. J. Zega, R. M. Stroud, T. Schull and K. E. Swider-Lyons, *J. Electrochem. Soc.*, 2008, **155**, B1314.
11. K. Sasaki, L. Zhang and R. R. Adzic, *Phys. Chem. Chem. Phys.*, 2008, **10**, 159-167.
12. M. A. Scibioh, S.-K. Kim, E. A. Cho, T.-H. Lim, S.-A. Hong and H. Y. Ha, *Appl. Catal. B*, 2008, **84**, 773-782.
13. X. Feng, Y. Shi and H. Zhou, *J. Rare Earth*, 2012, **30**, 29-33.
14. W. C. Chueh, Y. Hao, W. Jung and S. M. Haile, *Nat. Mater.*, 2012, **11**, 155-161.
15. M. A. Scibioh, S.-K. Kim, E. A. Cho, T.-H. Lim, S.-A. Hong and H. Y. Ha, *Appl. Catal. B*, 2008, **84**, 773-782.
16. Hariyanto, W. W. Purwanto, R. W. Seomantojo and U. Stimming, *J. Chem. Nat. Resour. Eng.*, 2007, **2**, 47-61.
17. H. B. Yu, J.-H. Kim, H.-I. Lee, M. A. Scibioh, J. Lee, J. Han, S. P. Yoon and H. Y. Ha, *J. Power Sources*, 2005, **140**, 59-65.
18. C. Xu and P. K. Shen, *Chem. Commun.*, 2004, 2238-2239.
19. C. Xu and P. K. Shen, *J. Power Sources*, 2005, **142**, 27-29.
20. S. Huang, C. Chang and C. Yeh, *J. Catal.*, 2006, **241**, 400-406.
21. Y. Zhou, C. L. Menendez, M. J. F. Guinel, E. C. Needels, I. Gonzalez-Gonzalez, D. L. Jackson, N. J. Lawrence, C. R. Cabrera and C. L. Cheung, *RSC Adv.*, 2014, **4**, 1270-1275.
22. C. L. Campos, C. Roldán, M. Aponte, Y. Ishikawa and C. R. Cabrera, *J. Electroanal. Chem.*, 2005, **581**, 206-215.
23. H. C. Yao and Y. F. Y. Yao, *J. Catal.*, 1984, **86**, 254-265.
24. V. Matolín, M. Cabala, I. Matolínová, M. Škoda, M. Václavů, K. C. Prince, T. Skála, T. Mori, H. Yoshikawa, Y. Yamashita, S. Ueda and K. Kobayashi, *Fuel Cells*, 2010, **10**, 139-144.
25. Y. H. Lin, X. L. Cui, C. H. Yen and C. M. Wai, *Langmuir*, 2005, **21**, 11474-11479.
26. A. Trovarelli, ed., *Catalysis by Ceria and Related Materials*, ICP, London, 2002.
27. J. Xu, J. Harmer, G. Li, T. Chapman, P. Collier, S. Longworth and S. C. Tsang, *Chem. Commun.*, 2010, **46**, 1887-1889.
28. N. J. Lawrence, J. R. Brewer, L. Wang, T.-S. Wu, J. M. Wells-Kingsbury, M. M. Ihrig, G. Wang, Y.-L. Soo, W.-N. Mei and C. L. Cheung, *Nano Lett.*, 2011, **11**, 2666-2671.
29. Y. J. Guan, D. A. J. M. Ligthart, O. Pirgon-Galin, J. A. Z. Pieterse, R. A. van Santen and E. J. M. Hensen, *Top. Catal.*, 2011, **54**, 424-438.
30. S. Chauhan, G. J. Richards, T. Mori, P. Yan, J. P. Hill, K. Ariga, J. Zou and J. Drennan, *J. Mater. Chem. A*, 2013, **1**, 6262-6270.
31. S. K. Meher and G. R. Rao, *ACS Catal.*, 2012, **2**, 2795-2809.
32. D. R. Ou, T. Mori, K. Fugane, H. Togasaki, F. Ye and J. Drennan, *J. Phys. Chem. C*, 2011, **115**, 19239-19245.
33. J. M. Anderson, J. Patel, A. S. Karakoti, N. Greeneltch, D. J. Díaz and S. Seal, *Electrochim. Acta*, 2011, **56**, 2541-2545.
34. C. Xu, R. Zeng, P. K. Shen and Z. Wei, *Electrochim. Acta*, 2005, **51**, 1031-1035.
35. A. Varez, E. Garcia-Gonzalez and J. Sanz, *J. Mater. Chem.*, 2006, **16**, 4249-4256.
36. Q. Fu, H. Saltsburg and M. Flytzani-Stephanopoulos, *Science*, 2003, **301**, 935-938.
37. K. Fugane, T. Mori, D. R. Ou, A. Suzuki, H. Yoshikawa, T. Masuda, K. Uosaki, Y. Yamashita, S. Ueda, K. Kobayashi, N. Okazaki, I. Matolinova and V. Matolin, *Electrochim. Acta*, 2011, **56**, 3874-3883.
38. J. P. W. Scharlemann and W. F. Laurance, *Science*, 2008, **319**, 43-44.

39. C. W. Xu, L. Q. Cheng, P. K. Shen and Y. L. Liu, *Electrochem. Commun.*, 2007, **9**, 997-1001.
40. M. Mogensen, N. M. Sammes and G. A. Tompsett, *Solid State Ionics*, 2000, **129**, 63-94.
41. H. Wang, A. Chroneos and U. Schwingenschlogl, *J. Chem. Phys.*, 2013, **138**.
42. S. R. Wang, T. Kobayashi, M. Dokiya and T. Hashimoto, *J. Electrochem. Soc.*, 2000, **147**, 3606-3609.
43. M. Burbano, D. Marrocchelli and G. W. Watson, *J. Electroceram.*, 2014, **32**, 28-36.
44. Q. He, S. Mukerjee, B. Shyam, D. Ramaker, S. Parres-Esclapez, M. J. Illan-Gomez and A. Bueno-Lopez, *J. Power Sources*, 2009, **193**, 408-415.
45. K. Scott, E. Yu, G. Vlachogiannopoulos, M. Shivare and N. Duteanu, *J. Power Sources*, 2008, **175**, 452-457.

